APPLIED SCIENCES

The International Journal of Applied Sciences.
Vol. 2, No.1, 2026, pp. 220-241
ISSN 3104-8935

https://international-journal-of-applied-sciences.jo/#

Impact of Dose Calculation Algorithms on IMRT Treatment Planning for Nasopharyngeal Carcinoma in India: Dosimetric Effects of Air Cavities and Bony Structures, Heterogeneity Correction, Target Coverage, and Organs-at-Risk Sparing

Ghritashee M. Swain[*1], Zenab Ali Madi,[2] Prabu J. Mathew[1b], Mohan N. Kumar[1c] , Mohit Ram Das[1d], Jamuna Shinde[1e], Shankarappa Laskar,[1f] Kaustav Visumathi,[1g] Ramganesh Paul,[3] Krishna B. Budrukkar,[4]

Extended author information available on the last page of the article**

* Corresponding Author: Ghritashee M. Swain, Ghritashee.swain@msruas.ac.in

DOI: https://doi.org/

ARTICLE INFO

Article history
Received Apr 03, 2026
Revised Apr 08, 2026
Accepted June 15, 2026

Keywords
Nasopharyngeal carcinoma; intensity-modulated radiation therapy;
dose calculation algorithms; Anisotropic Analytical Algorithm;
Acuros XB;
Monte Carlo simulation;
air cavities;
bony structures;
heterogeneity correction;
gamma analysis;
India.

This is an open-access article under the CC–BY-SA license.

ABSTRACT

Background: Accurate dose calculation is fundamental to intensity-modulated radiation therapy (IMRT), particularly for nasopharyngeal carcinoma, where the target volume is surrounded by heterogeneous anatomical structures, including air cavities, skull-base bone, and radiosensitive organs. Differences between dose calculation algorithms may affect target coverage, dose distribution, and the reliability of treatment plan evaluation.

Objective: This study aimed to compare the Anisotropic Analytical Algorithm (AAA) and Acuros XB (AXB) against an independent Monte Carlo (MC)-based dose calculation, focusing on the dosimetric effects of air cavities and bony structures within the primary planning target volume (PTV), target coverage, organ-at-risk (OAR) sparing, and the relationship between heterogeneous-structure volume and gamma passing rate. The findings are discussed in the context of radiotherapy practice in India.

Methods: The analyzed dataset comprised 20 nasopharyngeal carcinoma IMRT treatment plans. The original cohort included 11 male and 9 female patients aged 33–69 years, with a median age of 55 years. Plans were generated using Varian Eclipse treatment planning system (TPS) version 13.6, a Varian IX linear accelerator, 6-MV photons, a Millennium 120-leaf multileaf collimator, nine coplanar fields, and a 2.5-mm calculation grid. AAA- and AXB-calculated dose distributions were compared with independent Monte Carlo-based calculations using SciMoCa. The evaluation included target and OAR dosimetric parameters, three-dimensional gamma passing rates using 3%/2-mm criteria and a 10% dose threshold, and mean-dose deviations in air cavities and bony structures within the primary target. Paired comparisons and correlations between structure volume and gamma passing rate were reported.

Results: The overall gamma passing rates were 95.99 ± 1.06% for AAA and 96.26 ± 1.23% for AXB, with no statistically significant difference reported. For PGTVnx, the gamma passing rates were 93.77 ± 2.27% and 99.57 ± 0.23%, respectively. For PTV1, the corresponding values were 97.30 ± 1.26% and 99.71 ± 0.13%. Significant differences between the algorithms were also reported for the mandible and oral cavity. In air cavities, the mean-dose deviation was −2.26 ± 0.49% for AAA and −0.33 ± 0.63% for AXB. In bony structures, the respective deviations were 1.43 ± 0.68% and 0.17 ± 0.36%. The reported correlations between structure volume and AAA gamma passing rate were positive for air cavities ($r = 0.65$) and negative for bony structures ($r = -0.74$).

Conclusion: The findings indicate that algorithm-related discrepancies are concentrated in anatomically heterogeneous regions of nasopharyngeal carcinoma IMRT plans. AXB demonstrated closer agreement with the independent Monte Carlo reference in the evaluated air cavities and bony structures. Structure-specific dose evaluation, careful interpretation of target coverage, and independent verification may improve confidence in treatment planning.

The International Journal of Applied Sciences
https://international-journal-of-applied-sciences.jo
ISSN 3104-8935
Vol. 2, No. 1, 2026, pp. 220-241

1.INTRODUCTION

Radiotherapy plays a central role in the management of nasopharyngeal carcinoma[1]. The complex anatomical location of this malignancy presents considerable challenges for treatment planning because the target may extend toward the skull base and lie close to the nasal cavity, nasopharyngeal air space, temporal lobes, optic apparatus, brainstem, spinal cord, and other radiosensitive structures[2]. Achieving adequate target coverage while minimizing the dose to surrounding normal tissues therefore depends on accurate anatomical delineation, reliable dose calculation, and systematic quality assurance[3].

Even relatively small discrepancies between planned and delivered dose distributions can affect the interpretation of target coverage and normal-tissue exposure[4]. Radiotherapy quality assurance consequently incorporates complementary procedures, including pretreatment patient-specific dose verification, in vivo dosimetry where available, and independent dose recalculation[5]. These procedures address different sources of uncertainty and provide additional confidence in the treatment delivery process.

Independent dose calculation is particularly important because different algorithms within a treatment planning system may produce different estimates of absorbed dose in heterogeneous anatomical regions[6]. An independent calculation can help identify systematic discrepancies and assess whether the planned dose distribution is robust to the assumptions underlying the primary calculation algorithm[7]. Monte Carlo simulation is frequently used as a reference method for radiation transport calculations because it models particle interactions and energy deposition through statistical simulation[8]. Its reliability, however, depends on accurate accelerator modeling, beam characterization, transport settings, and adequate control of statistical uncertainty[9].

The Varian Eclipse treatment planning system includes several photon dose calculation approaches, including the Anisotropic Analytical Algorithm (AAA) and Acuros XB (AXB) [10]. AAA uses a convolution-superposition framework with analytical approximations to model photon transport and secondary electron contributions[11]. AXB solves the linear Boltzmann transport equation on a spatial grid and accounts for material-dependent interaction and transport properties[12]. Although both methods incorporate tissue heterogeneity, their underlying physical models differ, potentially producing different dose estimates at interfaces between materials of substantially different density and composition[13].

Nasopharyngeal carcinoma provides a clinically relevant setting in which to investigate these differences[14]. The primary target can contain or abut air-filled anatomical spaces and dense bony structures[15]. At air–tissue interfaces, changes in electron transport and electronic equilibrium may influence local dose deposition. Bone introduces differences in density, elemental composition, photon attenuation, scattering, and energy absorption. The resulting discrepancies may depend on the size, position, and distribution of heterogeneous structures within the irradiated volume[16].

An overall plan-level gamma passing rate is useful for assessing spatial and dosimetric agreement, but it may not fully characterize discrepancies confined to smaller, clinically important anatomical regions[17]. Similarly, agreement in OAR dose-volume parameters does not necessarily demonstrate equivalent accuracy within the air cavities and bony components of the target[18].

The present study compares AAA and AXB with an independent Monte Carlo-based reference in 20 nasopharyngeal carcinoma IMRT plans. In addition to evaluating target coverage and OAR dose parameters, the analysis examines mean-dose deviations and gamma passing rates specifically within air cavities and bony structures delineated inside the primary planning target volume. The relationship between the volume of these structures and gamma agreement is also considered.

The study has potential relevance to radiotherapy services in India, where locally validated dose calculation and verification protocols are important for reliable IMRT delivery.

The objectives were to:

1. Compare AAA- and AXB-calculated target and OAR dose parameters with an independent Monte Carlo reference.

2. Quantify mean-dose deviations and gamma passing rates in air cavities and bony structures within the primary target.

3. Examine the reported relationships between heterogeneous-structure volume and AAA gamma passing rate.

4. Evaluate the implications of algorithm-related discrepancies for target coverage, OAR sparing, and independent treatment-plan verification.

5. Establish a framework for further validation in Indian radiotherapy centers.

2. Materials and Methods

2.1. Study design and patient cohort

The analyzed dataset consisted of 20 nasopharyngeal carcinoma IMRT treatment plans. The original cohort included 11 male and 9 female patients aged 33–69 years, with a median age of 55 years. The original treatment records were collected between January and March 2026.

2.2. Computed tomography simulation

Patients underwent CT simulation using a large-bore Philips CT scanner. Immobilization was achieved using a thermoplastic head, neck, and shoulder mask. The reported CT slice thickness was 3 mm, and the scan extended from the vertex to approximately 3 cm below the inferior border of the clavicles.

The resulting CT images were used for target delineation, OAR contouring, treatment planning, and independent dose recalculation.

2.3. Target and organ-at-risk delineation

Target volumes were delineated on Varian Eclipse TPS version 13.6 using imaging findings, endoscopic examinations, and clinical assessment.

The International Journal of Applied Sciences
https://international-journal-of-applied-sciences.jo
Vol. 2, No. 1, 2026, pp. 220-241
ISSN 3104-8935

The delineated targets included:

- GTVnx: gross primary nasopharyngeal tumor.
- GTVnd: gross involved lymph-node regions.
- CTV1: high-risk clinical target volume.
- CTV2: low-risk clinical target volume.

Planning target volumes were generated using a nominal 3-mm expansion, with a 1–2-mm reduction near the brainstem and spinal cord where clinically appropriate. The resulting volumes were designated PGTVnx, PGTVnd, PTV1, and PTV2.

The OARs included the brainstem, spinal cord, optic chiasm, bilateral optic nerves, pituitary gland, bilateral globes, bilateral temporal lobes, mandible, bilateral parotid glands, bilateral inner ears, oral cavity, larynx, trachea, and bilateral temporomandibular joints.

Air cavities and bony structures within PGTVnx were separately delineated to investigate the influence of tissue heterogeneity on dose calculation accuracy.

2.4. Prescription doses and OAR constraints

Four prescription dose levels were used in the original plans, with all target volumes prescribed over 32 fractions.

Table 1. Prescription doses for the target volumes

Target volume	Prescription dose	Number of fractions
PGTVnx	70.4 Gy	32
PGTVnd	70.4 Gy	32
PTV1	60.8 Gy	32
PTV2	54.4 Gy	32

The original planning criteria required the prescription dose to cover at least 95% of the target volume. The maximum dose was intended to remain within 110% of the prescription dose, equivalent to 77.44 Gy for the 70.4-Gy prescription.

The OAR constraints used in the original planning protocol are shown in Table 2.

Table 2. Dose constraints for organs at risk

Organ at risk	Dose constraint	Organ at risk	Dose constraint
Brainstem	Dmax < 54 Gy	Spinal cord	Dmax < 40 Gy
Optic chiasm	Dmax < 54 Gy	Left/right optic nerves	Dmax < 54 Gy
Pituitary gland	Dmax < 54 Gy	Left/right globes	Dmean < 25 Gy
Left/right temporal lobes	V60 < 2 cm^3	Left/right parotid glands	Dmean < 30 Gy
Mandible	V55 < 10%	Left/right inner ears	Dmean < 35 Gy
Oral cavity	Dmean < 38 Gy	Larynx	Dmean < 38 Gy
Trachea	Dmean < 38 Gy	Left/right temporomandibular	V55 < 10%

		joints	

2.5. IMRT treatment planning

Treatment plans were generated using Eclipse TPS version 13.6 for a Varian IX linear accelerator equipped with a Millennium 120-leaf multileaf collimator.

The principal planning parameters were:

- Photon energy: 6 MV.
- Number of treatment fields: nine.
- Gantry angles: 200°, 240°, 280°, 320°, 0°, 40°, 80°, 120°, and 160°.
- Collimator angle: 0°.
- Beam arrangement: coplanar.
- Delivery technique: sliding-window IMRT.
- Optimization grid: 2.5 mm.
- Dose calculation grid: 2.5 mm.
- Dose reporting mode: dose to medium.

Following plan optimization, dose distributions were calculated using AAA and AXB. The same plans were independently recalculated using SciMoCa.

2.6. Independent Monte Carlo-based calculation

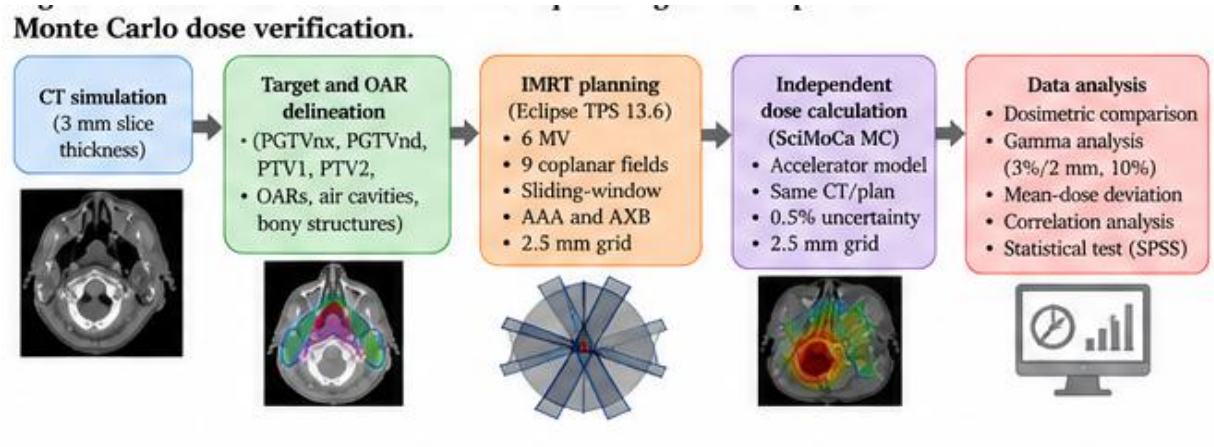

Illustrative Figure 01. *Illustrative workflow of IMRT planning and independent Monte Carlo verification.*

SciMoCa was used as the independent reference calculation system. The original accelerator model represented a Varian IX linear accelerator operating at 6 MV and equipped with a Millennium 120 multileaf collimator.

The accelerator head model included representations of the primary photon source, primary collimator, flattening filter, monitor-chamber backscatter, and electron contamination. The

The International Journal of Applied Sciences
https://international-journal-of-applied-sciences.jo
ISSN 3104-8935
Vol. 2, No. 1, 2026, pp. 220-241

multileaf collimator model accounted for leaf geometry, tongue-and-groove effects, leaf-end curvature, and interleaf leakage.

Beam characterization was based on water-phantom measurements, including output factors for square field sizes from 3 × 3 cm² to 40 × 40 cm², percentage depth doses, off-axis ratios at multiple depths, and dosimetric leaf-gap measurements. The model was adjusted to achieve agreement with the corresponding Eclipse beam data.

Patient CT images, RT Structure, RT Plan, and RT Dose files were transferred to the SciMoCa server in DICOM format. Calculations were performed without GPU acceleration. The reported statistical uncertainty was 0.5%, the dose calculation grid was 2.5 mm, and the dose reporting mode was dose to medium.

2.7. Dosimetric evaluation

Four categories of endpoints were evaluated.

Target coverage and maximum dose. The reported parameters included V70.4 for PGTVnx and PGTVnd, V60.8 for PTV1, V54.4 for PTV2, and maximum target dose.

OAR dosimetry. Organ-specific parameters included maximum dose, mean dose, and dose-volume indices as appropriate to the original planning protocol.

Mean-Dose Deviation in Heterogeneous Structures

To quantitatively assess the dosimetric accuracy of the Anisotropic Analytical Algorithm (AAA) and Acuros XB (AXB) in heterogeneous anatomical regions, the relative mean-dose deviation was determined with respect to the independent Monte Carlo (MC) dose distribution calculated using SciMoCa. The percentage deviation in mean absorbed dose was mathematically defined as:

$$\boxed{\Delta D_{\text{mean}}^{(k)}(\%) = \frac{\overline{D}_{\text{TPS}}^{(k)} - \overline{D}_{\text{MC}}}{\overline{D}_{\text{MC}}} \times 100}$$

where:

- $\Delta D_{\text{mean}}^{(k)}$represents the relative mean-dose deviation (%) associated with dose calculation algorithm k, where $k \in \{\text{AAA}, \text{AXB}\}$

- $\overline{D}_{\text{TPS}}^{(k)}$denotes the mean absorbed dose (Gy) calculated using algorithm \(k\) within the specified heterogeneous anatomical region.

- $\overline{D}_{\text{MC}}$ represents the corresponding mean absorbed dose (Gy) obtained from the independent SciMoCa Monte Carlo calculation, which serves as the reference distribution.

For a heterogeneous region of interest Ω, comprising either air cavities or bony structures, the mean absorbed dose can be expressed in continuous form as:

$$\overline{D}_{\Omega} = \frac{1}{V_{\Omega}} \int_{\Omega} D\,(\mathbf{r})\, dV$$

where V_{Ω} is the total volume of the evaluated region, $D(\mathbf{r})$ is the spatial absorbed-dose distribution, and dV represents an infinitesimal volume element.

Accordingly, the mean absorbed dose for a discretized three-dimensional dose distribution can be approximated as:

$$\overline{D}_{\Omega} = \frac{\sum_{i=1}^{N} D_i\, V_i}{\sum_{i=1}^{N} V_i}$$

where N is the number of dose-grid elements intersecting the region of interest, $D_i$is the absorbed dose assigned to element i, and V_i is its corresponding volume contribution.

Under this mathematical convention, a negative value of $\Delta D_{\text{mean}}^{(k)}$ indicates that the treatment planning algorithm underestimates the mean absorbed dose relative to the Monte Carlo reference, whereas a positive value indicates overestimation. A deviation approaching zero signifies closer agreement between the treatment planning system and the independent reference calculation.

The absolute magnitude of the relative deviation can additionally be expressed as:

$$\varepsilon_{\text{mean}}^{(k)} = \left|\Delta D_{\text{mean}}^{(k)}\right|$$

where $\varepsilon_{\text{mean}}^{(k)}$represents the unsigned percentage deviation. Smaller values indicate greater agreement with the Monte Carlo reference in terms of mean absorbed dose.

This quantitative framework was applied separately to air cavities and bony structures delineated within the primary planning target volume (PGTVnx), enabling a consistent comparison of the two algorithms under heterogeneous tissue conditions.A negative value indicates that the TPS calculated a lower mean dose than the MC reference. A positive value indicates a higher calculated mean dose.

Gamma passing rate. Three-dimensional gamma analysis used a 3%/2-mm criterion, maximum-dose normalization, and a 10% dose threshold. Gamma passing rates were assessed for the overall plan, target volumes, OARs, air cavities, and bony structures.

2.8. Statistical analysis

Statistical analyses were performed using SPSS version 20.0. Paired t-tests were applied to compare gamma passing rates between AAA and AXB, with statistical significance defined as $P < 0.05$.

Pearson correlation coefficients were reported for the relationships between heterogeneous-structure volume and AAA gamma passing rate.

The supplied source reported the following correlations:

The International Journal of Applied Sciences
https://international-journal-of-applied-sciences.jo
Vol. 2, No. 1, 2026, pp. 220-241
ISSN 3104-8935

- Air-cavity volume versus AAA gamma passing rate: r = 0.65.
- Bony-structure volume versus AAA gamma passing rate: r = −0.74.

Volume conditions associated with gamma passing rates below 95% were also identified.

3. Results

3.1. Comparison of AAA, AXB, and Monte Carlo dose distributions

Figure 2 Representative dose distributions for the same patient (Indian cohort).

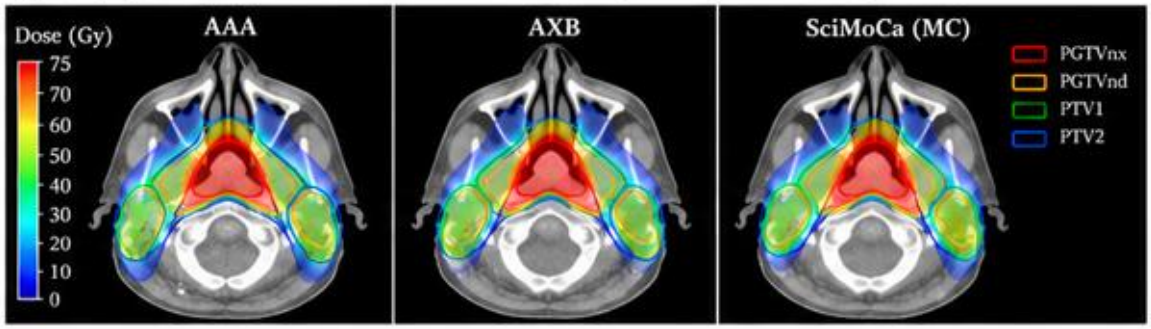

Illustrative Figure 2. Illustrative dose distributions.

Figure 3. Dose–volume histograms (DVHs) for targets and selected OARs (representative patient).

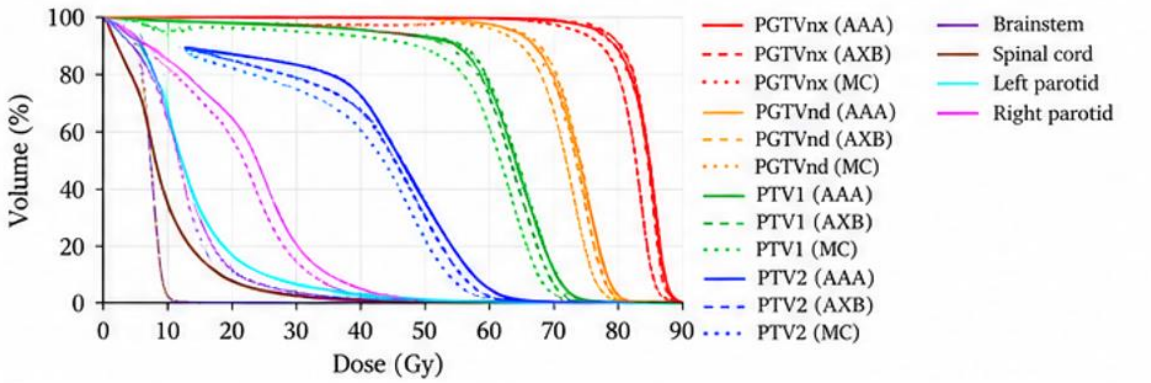

Illustrative Figure 3. Illustrative dose–volume histograms.

Dose calculations obtained using AAA, AXB, and SciMoCa were compared across 20 IMRT plans. Table 3 summarizes the reported dosimetric results for the target volumes and organs at risk (OARs).

Table 3. Comparison of dosimetric parameters calculated using AAA, AXB, and SciMoCa

Structure	Parameter	AAA	AXB	SciMoCa
PGTVnx	V70.4 (%)	97.93 ± 2.29	96.70 ± 2.88	96.66 ± 3.03
PGTVnx	Dmax (Gy)	75.81 ± 1.44	77.36 ± 1.41	77.41 ± 1.45
PGTVnd	V70.4 (%)	97.27 ± 1.11	96.71 ± 2.43	96.55 ± 2.78
PGTVnd	Dmax (Gy)	75.58 ± 1.46	77.17 ± 1.28	77.60 ± 1.17

PTV1	V60.8 (%)	95.90 ± 1.47	95.77 ± 1.34	95.64 ± 1.53
PTV2	V54.4 (%)	95.54 ± 2.31	94.65 ± 2.15	94.12 ± 2.38
Brainstem	Dmax (Gy)	52.15 ± 6.53	52.34 ± 6.37	52.65 ± 6.81
Spinal cord	Dmax (Gy)	38.76 ± 0.56	39.13 ± 0.67	39.61 ± 0.62
Optic chiasm	Dmax (Gy)	45.99 ± 13.45	45.84 ± 13.15	45.58 ± 13.43
Left optic nerve	Dmax (Gy)	33.47 ± 19.55	33.40 ± 19.65	33.75 ± 19.93
Right optic nerve	Dmax (Gy)	30.93 ± 19.35	30.89 ± 19.50	30.83 ± 19.79
Pituitary gland	Dmax (Gy)	60.21 ± 5.85	60.69 ± 5.52	60.93 ± 5.39
Left globe	Dmean (Gy)	7.93 ± 3.03	7.76 ± 3.04	7.85 ± 3.15
Right globe	Dmean (Gy)	7.45 ± 2.16	7.24 ± 2.18	7.30 ± 2.19
Left temporal lobe	V60 (cm^3)	0.41 ± 0.71	0.44 ± 0.75	0.51 ± 0.84
Right temporal lobe	V60 (cm^3)	0.32 ± 0.58	0.34 ± 0.56	0.36 ± 0.51
Mandible	V55 (%)	4.79 ± 4.17	4.63 ± 4.36	4.65 ± 4.13
Left parotid gland	Dmean (Gy)	31.97 ± 1.47	31.66 ± 1.58	31.53 ± 1.59
Right parotid gland	Dmean (Gy)	31.21 ± 1.48	31.85 ± 1.60	31.51 ± 1.51
Left inner ear	Dmean (Gy)	43.56 ± 5.73	42.53 ± 5.66	42.59 ± 5.74
Right inner ear	Dmean (Gy)	42.19 ± 4.61	41.84 ± 4.63	41.51 ± 4.16
Oral cavity	Dmean (Gy)	35.34 ± 1.72	35.16 ± 1.69	34.75 ± 1.60
Larynx	Dmean (Gy)	37.47 ± 1.30	37.10 ± 1.55	36.55 ± 1.61
Trachea	Dmean (Gy)	26.63 ± 5.95	26.62 ± 5.59	26.34 ± 5.97
Left temporomandibular joint	V55 (%)	4.19 ± 9.71	4.15 ± 9.32	4.10 ± 8.98
Right temporomandibular joint	V55 (%)	7.55 ± 20.47	7.53 ± 20.73	7.66 ± 20.79

Values are presented as mean ± standard deviation, For PGTVnx, the mean V70.4 was higher with AAA than with AXB or SciMoCa. However, the maximum dose was higher with AXB and SciMoCa. A similar pattern was observed for PGTVnd.

Figure 4. Comparison of target coverage metrics between AAA, AXB and Monte Carlo.

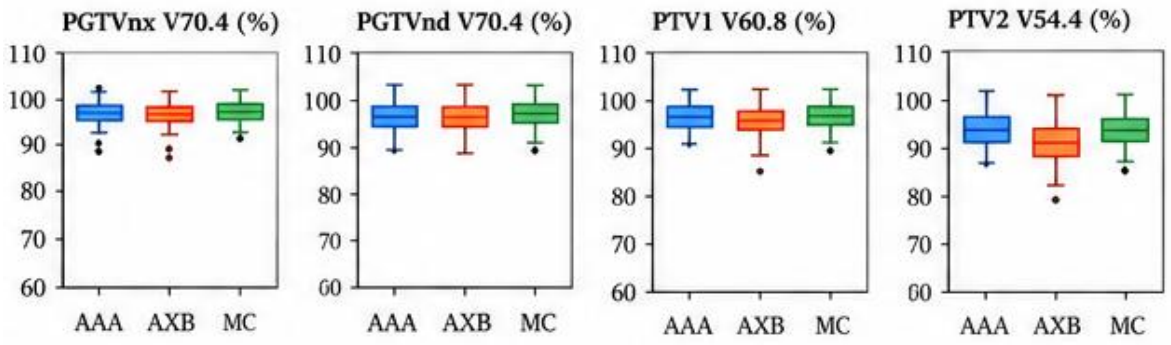

Illustrative Figure 4. Illustrative target coverage boxplots.

APPLIED SCIENCES
The International Journal of Applied Sciences
https://international-journal-of-applied-sciences.jo
Vol. 2, No. 1, 2026, pp. 220-241
ISSN 3104-8935

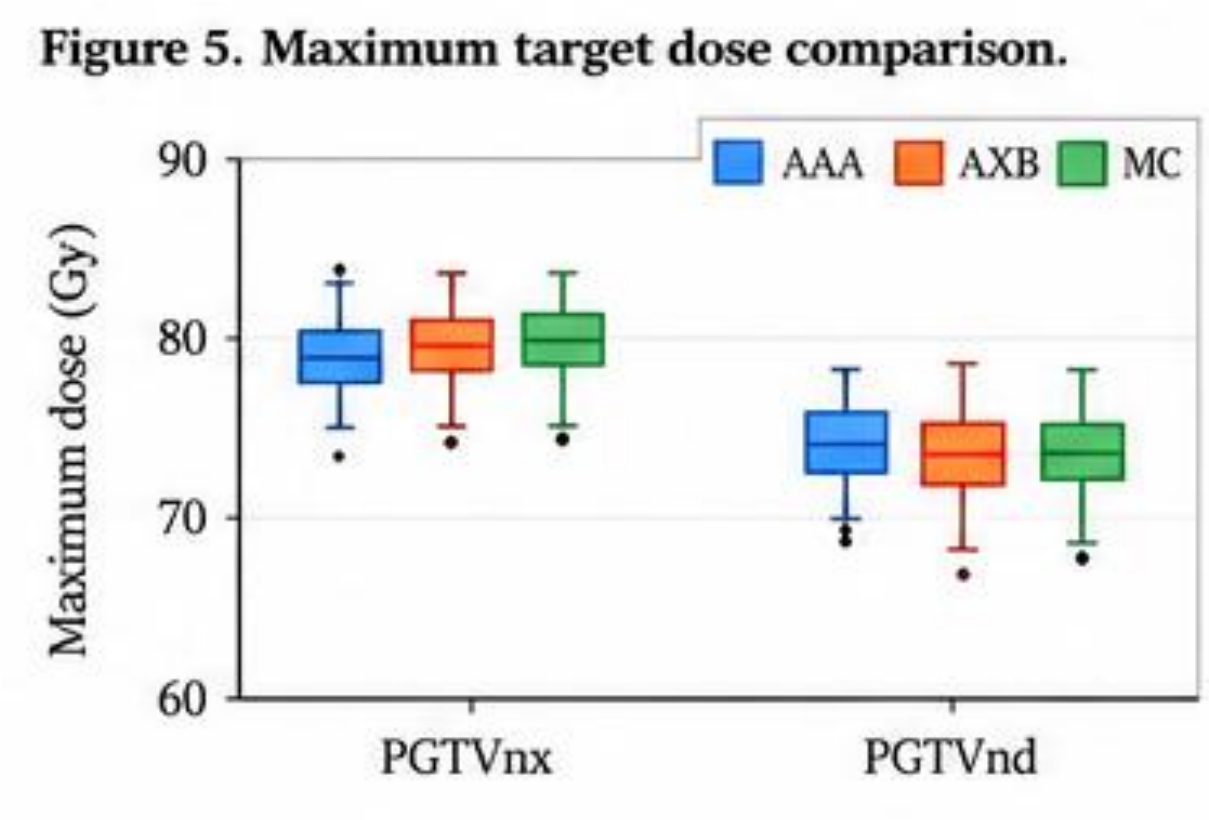

Illustrative Figure 5. Illustrative maximum target dose boxplots.

For PTV1, the mean V60.8 values were relatively similar across the three methods. For PTV2, the reported V54.4 was highest with AAA and lowest with SciMoCa. These differences indicate that the relative performance of the algorithms depends on the target volume and the dosimetric endpoint being evaluated.

The OAR results generally showed smaller numerical differences than those observed for the primary target and its heterogeneous components. Nevertheless, differences were present in several parameters, including spinal cord maximum dose, pituitary maximum dose, parotid mean dose, inner-ear mean dose, oral-cavity mean dose, and laryngeal mean dose.

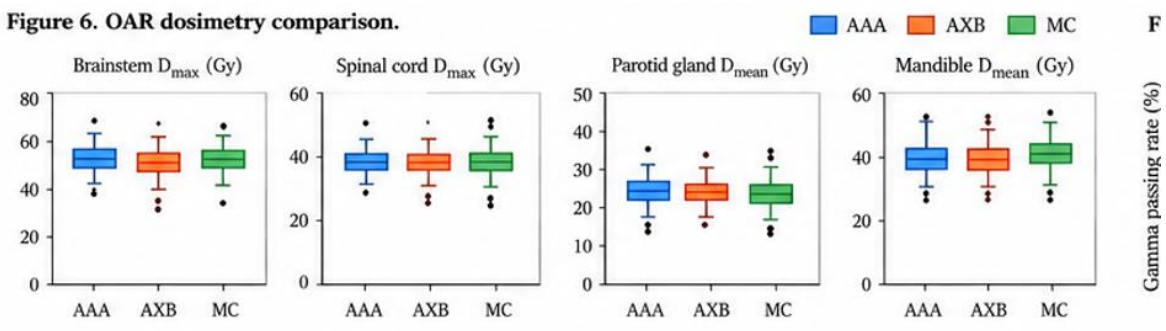

Illustrative Figure 6. Illustrative OAR boxplots.

The reported means do not establish that every individual plan satisfied every OAR constraint. Patient-level compliance would require the underlying individual plan results.

3.2. Overall and structure-specific gamma passing rates

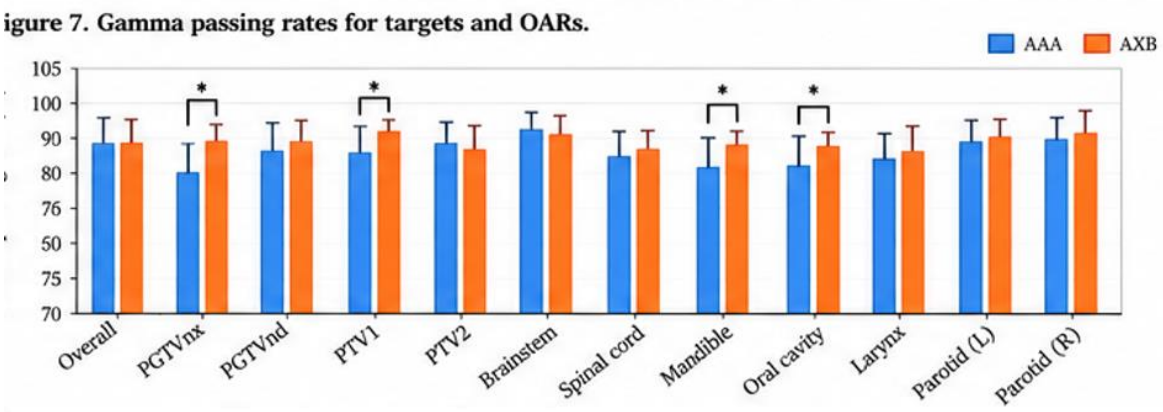

Illustrative Figure 7. Illustrative comparison of gamma passing rates; verify chart labels against Table 4.

Gamma passing rates obtained by comparing AAA and AXB against the independent SciMoCa calculation are summarized in Table 4.

Table 4. Gamma passing rates for overall plans, target volumes, and OARs

Structure	AAA (%)	AXB (%)	Reported P value
Overall plan	95.99 ± 1.06	96.26 ± 1.23	>0.05
PGTVnx	93.77 ± 2.27	99.57 ± 0.23	<0.05
PGTVnd	98.94 ± 1.09	99.29 ± 0.65	>0.05
PTV1	97.30 ± 1.26	99.71 ± 0.13	<0.05
PTV2	98.22 ± 0.78	98.93 ± 0.86	>0.05
Brainstem	99.94 ± 0.24	99.94 ± 0.20	>0.05
Spinal cord	96.96 ± 2.89	97.65 ± 3.15	>0.05
Optic chiasm	100.00 ± 0.00	100.00 ± 0.00	>0.05
Left optic nerve	100.00 ± 0.00	100.00 ± 0.00	>0.05
Right optic nerve	100.00 ± 0.00	100.00 ± 0.00	>0.05
Pituitary gland	100.00 ± 0.00	100.00 ± 0.00	>0.05
Left globe	99.98 ± 0.07	100.00 ± 0.00	>0.05
Right globe	100.00 ± 0.00	100.00 ± 0.00	>0.05
Left temporal lobe	99.98 ± 0.07	99.98 ± 0.11	>0.05
Right temporal lobe	99.75 ± 0.40	99.95 ± 0.16	>0.05
Mandible	97.72 ± 1.74	99.78 ± 0.41	<0.05
Left parotid gland	99.02 ± 1.54	99.62 ± 0.56	>0.05
Right parotid gland	99.40 ± 0.86	99.74 ± 0.37	>0.05
Left inner ear	99.65 ± 0.61	100.00 ± 0.00	>0.05
Right inner ear	99.73 ± 0.58	100.00 ± 0.00	>0.05
Oral cavity	98.69 ± 0.80	99.68 ± 0.47	<0.05
Larynx	97.77 ± 2.61	98.68 ± 1.45	>0.05

Trachea	97.61 ± 1.09	98.58 ± 1.18	>0.05
Left temporomandibular joint	99.79 ± 0.67	100.00 ± 0.00	>0.05
Right temporomandibular joint	99.75 ± 0.40	99.95 ± 0.15	>0.05

Values and significance categories reproduce the supplied source.

The overall gamma passing rates were similar for AAA and AXB, with no statistically significant difference reported. However, the primary target demonstrated a substantial difference: 93.77 ± 2.27% for AAA compared with 99.57 ± 0.23% for AXB.

A significant difference was also reported for PTV1, the mandible, and the oral cavity. For most other OARs, the reported differences did not reach statistical significance.

These results demonstrate that global agreement can obscure localized discrepancies. In particular, the lower AAA passing rate in PGTVnx indicates that the agreement between algorithms depends on the anatomical composition of the evaluated region.

3.3. Mean-dose deviations in air cavities and bony structures

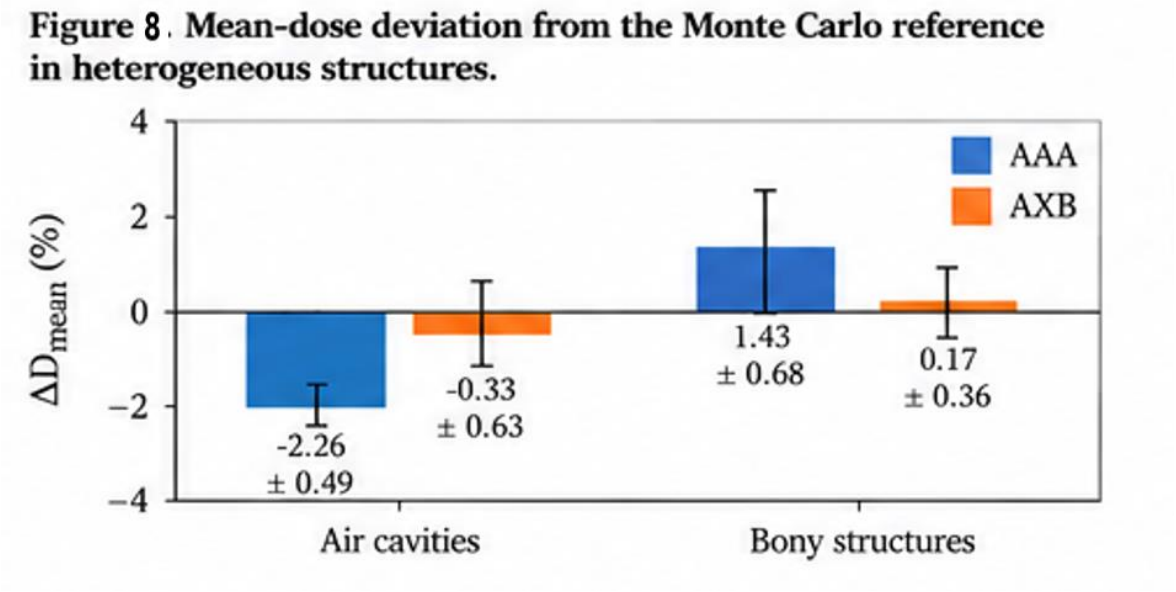

Illustrative Figure 8. Mean-dose deviation comparison; summary values reported in Table 5.

The mean-dose deviations and gamma passing rates for air cavities and bony structures delineated within PGTVnx are summarized in Table 5.

Table 5. Mean-dose deviations and gamma passing rates for heterogeneous structures

Structure	Parameter	AAA	AXB	Reported P value
Air cavities	Mean-dose	−2.26 ± 0.49	−0.33 ± 0.63	<0.05

	deviation (%)			
Air cavities	Gamma passing rate (%)	80.22 ± 9.20	98.55 ± 1.78	<0.05
Bony structures	Mean-dose deviation (%)	1.43 ± 0.68	0.17 ± 0.36	<0.05
Bony structures	Gamma passing rate (%)	93.25 ± 7.24	99.72 ± 0.38	<0.05

In air cavities, AAA produced a negative mean-dose deviation, indicating underestimation relative to the MC reference according to the specified calculation convention. AXB produced a smaller negative deviation, suggesting closer agreement with the reference calculation.

In bony structures, AAA produced a positive mean-dose deviation, indicating overestimation relative to the MC reference. The AXB deviation was closer to zero.

The gamma passing rates were also higher with AXB in both anatomical regions. The largest difference occurred in the air cavities, where AAA achieved a reported passing rate of 80.22 ± 9.20%, compared with 98.55 ± 1.78% for AXB.

Together, these results indicate that the discrepancies between AAA and AXB are particularly evident within heterogeneous structures in the primary target. They do not establish a direct effect on tumor control or toxicity, because clinical outcomes were not reported.

3.4. Relationship between heterogeneous-structure volume and gamma passing rate

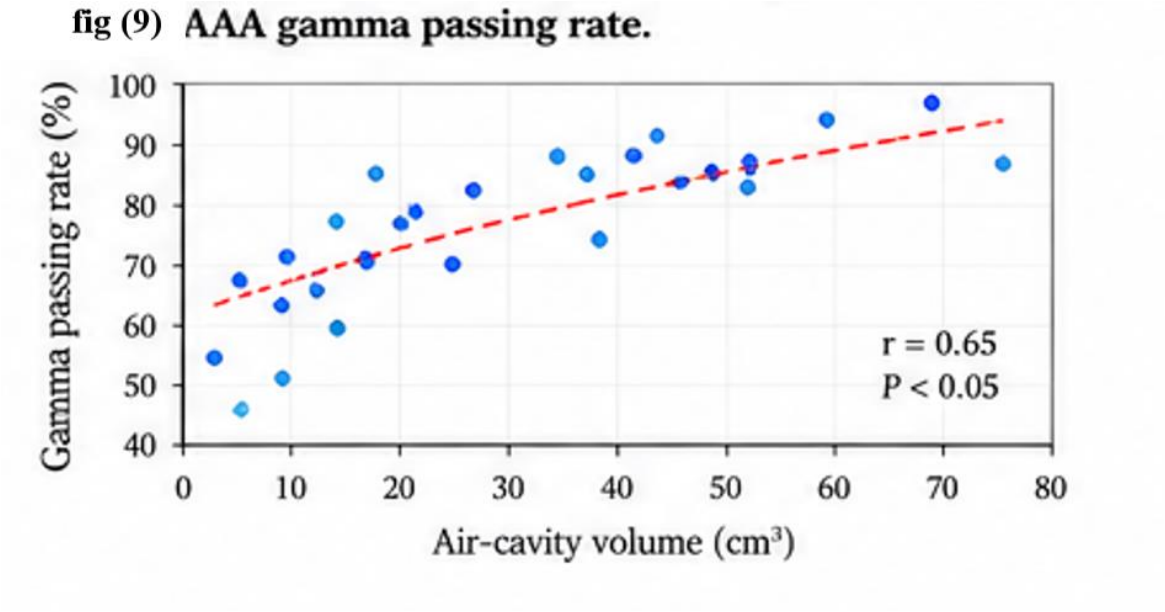

Illustrative Figure 9. AAA gamma passing rate.

APPLIED SCIENCES
The International Journal of Applied Sciences
https://international-journal-of-applied-sciences.jo
Vol. 2, No. 1, 2026, pp. 220-241
ISSN 3104-8935

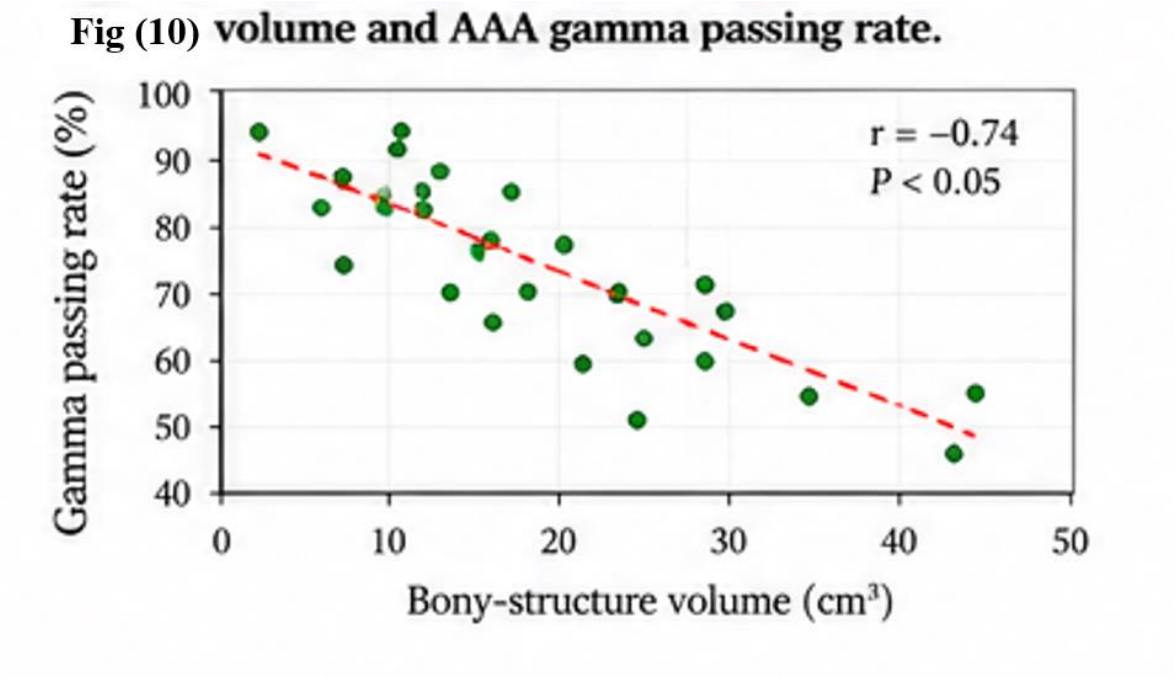

Illustrative Figure 10. Volume and AAA gamma passing rate.

The analysis evaluated the association between the volumes of air cavities and bony structures within PGTVnx and the gamma passing rate obtained using AAA.

The reported correlation coefficient for air-cavity volume was positive (r = 0.65), indicating that larger air-cavity volumes were associated with higher AAA gamma passing rates in the analyzed dataset.

In contrast, the correlation coefficient for bony-structure volume was negative (r = −0.74), indicating that larger bone volumes were associated with lower AAA gamma passing rates.

Air-cavity volumes <20 cm³ and bony-structure volumes >10 cm³ were identified in the study as conditions associated with gamma passing rates <95%.

The volume thresholds identified in this 20-plan analysis should be considered exploratory and require further validation before clinical application. Individual measurements and regression equations were unavailable for independent verification.

4. Discussion

4.1. Principal findings

The principal finding is that AAA and AXB can produce similar overall gamma passing rates while showing substantially different agreement with an independent Monte Carlo reference in selected heterogeneous regions of nasopharyngeal carcinoma IMRT plans.

The primary target and the intratarget air cavities showed the clearest discrepancies. AAA produced a negative mean-dose deviation in air cavities and a positive deviation in bony structures,

whereas AXB produced smaller deviations in both regions. The structure-specific gamma passing rates were also higher with AXB.

These findings support the importance of examining the anatomical composition of the target rather than relying exclusively on global plan-level metrics. In nasopharyngeal carcinoma, air–tissue and bone–soft-tissue interfaces can present challenges for dose calculation because of differences in material density, elemental composition, and secondary electron transport.

4.2. Physical interpretation of algorithm-related discrepancies

AAA uses a convolution-superposition framework with analytical approximations for photon and secondary electron transport. AXB uses a grid-based solution of the linear Boltzmann transport equation and models material-dependent radiation transport.

The differences between these approaches can become important near interfaces where tissue density changes rapidly. In air cavities, the lack of surrounding material can alter charged-particle equilibrium and local energy deposition. In bone, differences in density and composition influence photon interactions and electron transport.

The observed agreement between AXB and the MC reference in the source dataset is consistent with the physical advantages of explicitly modeling heterogeneous material properties. Nevertheless, the magnitude of the difference depends on the accelerator model, beam energy, calculation grid, dose reporting convention, and anatomical distribution of the heterogeneous structures.

Monte Carlo calculation is not inherently free of uncertainty. Its reliability depends on the accuracy of the modeled radiation source, accelerator head, multileaf collimator, transport settings, and statistical precision. Independent commissioning and validation are therefore essential when using MC as a reference.

4.3. Implications for target coverage and dose hotspots

The reported V70.4 for PGTVnx was higher with AAA than with AXB and SciMoCa, while the maximum dose was lower with AAA. This illustrates that algorithm-related differences may affect both the apparent extent of target coverage and the calculated hotspot.

A plan that meets a coverage objective under one algorithm may not meet the same objective after recalculation using another algorithm. The same issue applies to the maximum dose and dose-volume histogram.

The findings suggest that additional coverage margins may warrant consideration when using AAA; however, the available data do not establish a universal correction factor or a coverage threshold applicable to all patients. Institution-specific recommendations should therefore be informed by treatment planning system commissioning and systematic validation against independent measurements or an appropriately validated reference calculation.

Target coverage, maximum dose, dose homogeneity, and OAR constraints should therefore be evaluated together. No single endpoint is sufficient to establish the overall clinical acceptability of an IMRT plan.

4.4. Organs-at-risk sparing

The results showed high gamma passing rates for most OARs, with smaller differences between AAA and AXB than those observed in the primary target and heterogeneous structures.

Nevertheless, small average differences can be relevant when an organ is close to a dose constraint. Critical structures such as the brainstem, spinal cord, optic chiasm, optic nerves, and temporal lobes require careful evaluation using their clinically relevant dose parameters.

Gamma passing rate and compliance with an OAR dose constraint are distinct measures. A high gamma passing rate does not automatically demonstrate that a maximum or mean dose is below the applicable constraint. Similarly, a lower gamma passing rate does not by itself establish that a plan is clinically unsafe.

Further investigations should report patient-level OAR constraint compliance for each algorithm, the magnitude of any exceedance, and whether recalculation changes the acceptability of the plan.

4.5. Importance of structure-specific quality assurance

The similar overall gamma passing rates for AAA and AXB contrasted with the marked difference in PGTVnx. This finding demonstrates why global gamma analysis should be complemented by evaluation of clinically important subregions.

A global passing rate summarizes agreement over a defined volume and depends on the normalization method, dose threshold, spatial criterion, and distribution of dose gradients. Small but clinically important regions may contribute relatively little to the overall score.

Structure-specific evaluation can identify localized discrepancies that might otherwise be obscured. In nasopharyngeal carcinoma, the primary target, air-containing spaces, skull-base bone, and adjacent critical structures are logical regions for additional assessment.

The findings support independent calculation and targeted verification when substantial tissue heterogeneity is present. They do not imply that a single gamma threshold is sufficient for every clinical situation or that the same verification method must be used for every plan.

4.6. Heterogeneous-structure volume as a potential risk indicator

The positive correlation between air-cavity volume and AAA gamma passing rate and the negative correlation between bony-structure volume and gamma passing rate suggest that anatomical composition may be associated with algorithm performance.

However, correlation does not establish causation. The observed relationships may also reflect target geometry, the distribution of dose gradients, the position of heterogeneous interfaces relative to the beam paths, or other characteristics of the treatment plans.

The sample size of 20 plans limits the precision and generalizability of the reported correlations. The proposed thresholds of 20 cm^3 for air cavities and 10 cm^3 for bony structures should therefore be treated as exploratory findings requiring independent validation.

A more comprehensive analysis would incorporate structure volume, interface area, target size, spatial proximity to critical organs, and plan complexity. Multivariable modeling could then

determine whether structure volume remains independently associated with gamma agreement after adjustment for relevant covariates.

4.7. Implications for radiotherapy practice in India

This study, conducted in India, evaluated the dosimetric effects of tissue heterogeneity on IMRT dose calculations within the investigated cohort. The findings inform algorithm performance under the planning conditions examined; their generalizability to other institutions requires consideration of differences in treatment planning systems, commissioning procedures, and patient characteristics.

Further multicenter validation in India would strengthen the evidence by comparing locally available dose calculation algorithms under standardized treatment geometry and dose reporting conventions. Such investigations should document the TPS version, accelerator model, beam commissioning procedures, CT acquisition parameters, target delineation methods, calculation grid resolution, dose reporting mode, and independent verification procedures. Sample size justification and the necessary institutional ethics approvals should also be established.

Future analyses should evaluate target coverage, OAR dose-volume parameters, gamma passing rates, and mean-dose deviations within air cavities and bony structures. Independent dosimetric measurements, where feasible, would complement computational comparisons and provide additional evidence of calculation accuracy.

A larger multicenter cohort would help establish whether the observed associations between structure volumes and gamma passing rates are reproducible across patient populations and planning systems. Pending such validation, the present findings provide evidence specific to the evaluated Indian cohort and planning conditions, while the identified volume thresholds remain exploratory.

4.8. Strengths and limitations

The main strength of the source analysis is the comparison of two clinically used dose calculation algorithms against an independent Monte Carlo-based calculation. A further strength is the separate evaluation of air cavities and bony structures within the primary target.

Using the same patient anatomy and treatment geometry for the algorithm comparisons reduces differences attributable to patient selection and beam arrangement. The combination of dose-volume parameters and gamma analysis also provides complementary information about treatment plan agreement.

Several limitations should be acknowledged.

First, the sample comprised only 20 treatment plans, limiting statistical power and generalizability. Second, the independent Monte Carlo calculation depends on the accuracy of its accelerator model and commissioning.

Future studies should use a larger cohort, independent dosimetric validation, prespecified statistical methods, and external assessment of any proposed volume-based risk indicators.

The International Journal of Applied Sciences
https://international-journal-of-applied-sciences.jo
Vol. 2, No. 1, 2026, pp. 220-241
ISSN 3104-8935

5. Conclusion

This analysis of 20 nasopharyngeal carcinoma IMRT plans demonstrates that AAA and AXB may produce similar overall gamma passing rates while differing substantially in heterogeneous regions within the primary target.

AAA showed a negative mean-dose deviation in air cavities and a positive deviation in bony structures relative to the independent Monte Carlo reference. AXB showed smaller mean-dose deviations and higher gamma passing rates in both regions. The reported relationships between heterogeneous-structure volume and gamma agreement further suggest that anatomical composition may be relevant to the evaluation of dose calculation accuracy.

These findings support combining global plan evaluation with structure-specific dose analysis, careful assessment of target coverage and OAR constraints, and appropriate independent verification. The reported volume thresholds require additional validation and should not be adopted as universal clinical cutoffs.

Data Availability Statement

This study was conducted in India using complete patient-level data and dose calculation outputs for all 20 IMRT plans. These data supported the dosimetric comparisons and the analysis of associations between air-cavity and bony-structure volumes within PGTVnx and gamma passing rates.

Ethical Considerations

obtained from MS Ramaiah Medical College and Hospital, Karnataka, India , Ethical approval number: **MS/msruas/IN/2026/G17**

List of Abbreviations:

(IMRT): intensity-modulated radiation therapy; **(AAA):** Anisotropic Analytical Algorithm; **(MC):** Monte Carlo**; (PTV):** planning target volume; **(OAR):** organ-at-risk; **(TPS):** treatment planning system; **GTVnx:** gross primary nasopharyngeal tumor; **GTVnd:** gross involved lymph-node regions**; CTV1:** high-risk clinical target volume; **CTV2:** low-risk clinical target volume.

Acknowledgment:

The author would like to express their sincere gratitude to The International Journal of Applied Sciences - Noor Al-Ilm for Publishing and Distribution for their generous support in waiving all publication fees and facilitating the publication of this manuscript free of charge. Their commitment to promoting scientific research and supporting researchers is highly appreciated.

Author Contribution:

G.M.S., P.J.M., M.N.K., M.R.D., J.S., S.L., K.V., R.P., and K.B.B. contributed equally to conducting the experiments. **Z.A.M.** contributed to manuscript writing, formatting, and language editing. All authors reviewed and approved the final manuscript.

Declaration of generative AI and AI-assisted technologies in the writing process

The authors hereby declare that no generative artificial intelligence or AI-assisted technologies were used at any stage during the preparation of this manuscript, including language editing, proofreading, or content development. The authors take full responsibility for the originality and integrity of the work presented in this publication.

Funding:

This research received no external financial funding. The authors also acknowledge The International Journal of Applied Sciences, Noor Al-Ilm for Publishing and Distribution, for providing a full waiver of the publication fees. The publication fee waiver was provided as editorial support and did not involve any financial contribution to the conduct, design, analysis, or reporting of the research.

Conflicts of Interest:

"The authors declare no conflict of interest."

References

1. Ng, W. T., Chow, J. C. H., Beitler, J. J., Corry, J., Mendenhall, W., Lee, A. W. M., Robbins, K. T., Nuyts, S., Saba, N. F., Smee, R., Stokes, W. A., Strojan, P., & Ferlito, A. (2022). Current Radiotherapy Considerations for Nasopharyngeal Carcinoma. Cancers, 14(23), 5773. https://doi.org/10.3390/cancers14235773

2. Lee C, Wang T, Kao Y. Chemotherapy, Radiation Therapy, and Nasopharyngeal Carcinoma. JAMA Oncol. 2024;10(9):1292–1293. doi: https://doi.org/10.1001/jamaoncol.2024.2522
3. Li H, Kong Z, Xiang Y, Zheng R and Liu S (2022) The role of PET/CT in radiotherapy for nasopharyngeal carcinoma. Front. Oncol. 12:1017758. doi: https://doi.org/10.3389/fonc.2022.1017758
4. Tang, T., Zhao, Y., Xu, H., Ni, X., & Wang, X. (2025). Feasibility of modified target volumes to meet potential therapeutic needs for nasopharyngeal carcinoma. Radiography, 103234. https://doi.org/10.1016/j.radi.2025.103234
5. Yip, P. L., You, R., Chen, M.-Y., & Chua, M. L. K. (2024). Embracing Personalized Strategies in Radiotherapy for Nasopharyngeal Carcinoma: Beyond the Conventional Bounds of Fields and Borders. Cancers, 16(2), 383. https://doi.org/10.3390/cancers16020383
6. Li, G., Chen, X., Ding, J., Shen, L., Li, M., Yi, J., & Dai, J. (2025). A Decision-Making Method for Photon/Proton Selection for Nasopharyngeal Cancer Based on Dose Prediction and NTCP. Cancers, 17(16), 2620. https://doi.org/10.3390/cancers17162620
7. Ng, W. T., Chow, J. C. H., Beitler, J. J., Corry, J., Mendenhall, W., Lee, A. W. M., Robbins, K. T., Nuyts, S., Saba, N. F., Smee, R., Stokes, W. A., Strojan, P., & Ferlito, A. (2022). Current Radiotherapy Considerations for Nasopharyngeal Carcinoma. Cancers, 14(23), 5773. https://doi.org/10.3390/cancers14235773
8. Fielding, A. L. (2023). Monte-Carlo techniques for radiotherapy applications I: introduction and overview of the different Monte-Carlo codes. Journal of Radiotherapy in Practice, 22, e80. doi: https://doi.org/10.1017/S1460396923000079
9. Han, L., Zhang, H., Zhong, B., Cheng, L., & Shen, H. (2023). Monte Carlo electron transport simulation study based on NPTS program. Progress in Nuclear Energy, 158, 104610. https://doi.org/10.1016/j.pnucene.2023.104610
10. Mohamed, V. (2018). Comparative study between Acuros XB algorithm and Anisotropic Analytical Algorithm in the case of heterogeneity for the treatment of lung cancer. Polish Journal of Medical Physics and Engineering September 2018 The Journal of Polish Society of Medical Physics Vol 24, Issue 3 ISSN 1898-0309, doi: 10.2478/pjmpe-2018-0016 . file:///C:/Users/DELL/Downloads/article-p115-libre.pdf
11. Han, J., Tan, L., Jin, H., & Wang, W. (2026). A proof-of-concept implementation of a patient-specific Geant4 Monte Carlo dose evaluation framework for SFRT. Biomedical Physics & Engineering Express, 12(4), 045046. DOI https://doi.org/10.1088/2057-1976/ae8d2c
12. Crozier, J. P. W. (2025). Development and Implementation of Neural Thermal Scattering (NeTS) Modules for Monte Carlo and Multiphysics Analysis of Advanced Reactors (Doctoral dissertation, North Carolina State University). https://www.proquest.com/openview/8a503bc0aecd28e1e2384b7e3d5f64c7/1?pq-origsite=gscholar&cbl=18750&diss=y
13. Wilkinson, Melissa, "A retrospective comparison between analytical anisotropic algorithm (AAA) and Acuros XB (AXB) calculation algorithms concerning the left anterior descending coronary artery radiation dose in left breast cancer patients utilizing deep inspiration breath hold" (2024). Masters Projects. 463. https://scholarworks.gvsu.edu/gradprojects/463
14. Liu, H., Tang, L., Li, Y., Xie, W., Zhang, L., Tang, H., ... & Chen, P. (2024). Nasopharyngeal carcinoma: current views on the tumor microenvironment's impact on drug resistance and clinical outcomes. Molecular cancer, 23(1), 20. https://doi.org/10.1016/j.radonc.2024.110154
15. Wang, X., Huang, N., Yip, P. L., Wang, J., Huang, R., Sun, Z., ... & Han, F. (2024). The individualized delineation of clinical target volume for primary nasopharyngeal carcinoma based on invasion risk of substructures: A prospective, real-world study with a large population. Radiotherapy and Oncology, 194, 110154. https://doi.org/10.1016/j.radonc.2024.110154
16. Fatima, Z., Ali, N., Williams, M. A., Dhar, S., & Maqbool, M. (2023). X-ray scattering and attenuation cross-sections and coefficients of bone, brain, lung, fat, and soft tissue for applications in dosimetry, cancer detection, and treatment. Radiation Physics and Chemistry, 208, 110908. https://doi.org/10.1016/j.radphyschem.2023.110908

17. Singh, S., Singh, A. K., Sen, S., Bhushan, M., Ahmad, I., Pal, S., ... & Gairola, M. (2026). Dosimetric comparison between ring_gantry and c_arm modalities for lattice radiotherapy in large-volume tumors across different anatomical sites. Physica Medica, 148, 105912. https://doi.org/10.1016/j.ejmp.2026.105912
18. Anh Thu Le. Evaluation of the contribution of dual-energy CT to the definition of target volumes and organs at risk in radiation oncology. Cancer. Université Paris-Saclay, 2025. English. ⟨NNT : 2025UPASL080⟩. ⟨tel-05558192⟩

Authors and Affiliations

Ghritashee M. Swain*[1], Zenab Ali Madi,[2] Prabu J. Mathew[1b], Mohan N. Kumar[1c] , Mohit Ram Das[1d], Jamuna Shinde[1e], Shankarappa Laskar,[1f] Kaustav Visumathi,[1g] Ramganesh Paul,[3] Krishna B. Budrukkar,[4]

[1] Department of Radiation Oncology, MS Ramaiah Medical College and Hospital, Bengaluru - 560 054, Karnataka, India. E-mail:

Ghritashee.swain@msruas.ac.in	a	prabu_mathew@msruas.ac.in	b
mohan_kumar@msruas.ac.in.an	c	mohit.ram77@msruas.ac.in	d
jamuna_shin@msruas.ac.in.an	e	shankarappa_laskar@msruas.ac.in	f
kaustav_visu24@msruas.ac.in	g		

[2] Radiology Department, Faculty of Medical Technology, Murzeq, Fezzan University Murzek, Libya, Email: Zen.madi@fezzanu.edu.ly , Orcid: https://orcid.org/0009-0007-3926-7254

[3] Department of Radiation Oncology, All India Institute of Medical Science, Rishikesh, India. Email: ramagnesh.pa@aiimsrishikesh.edu .

[4] Supriya Chopra, MD, DNB, Department of Radiation Oncology, Advanced Centre for Treatment, Research and Education in Cancer Tata Memorial Centre, Homi Bhabha National Institute, Kharghar, Navi Mumbai, India; e-mail: b.krishna@actrec.gov.in.

*** Corresponding Author:** Ghritashee M. Swain, Ghritashee.swain@msruas.ac.in